magnetism

MDPI

Article

Coexistence of Long-Range Magnetic Order and Magnetic Frustration of a Novel Two-Dimensional $S = 1/2$ Structure: $Na_2Cu_3(SeO_3)_4$

Emily D. Williams [1], Keith M. Taddei [2], Kulugammana G. S. Ranmohotti [3], Narendirakumar Narayanan [4], Thomas Heitmann [4,5], Joseph W. Kolis [1] and Liurukara D. Sanjeewa [4,6,*]

1 Department of Chemistry and Center for Optical Materials Science and Engineering Technologies (COMSET), Clemson University, Clemson, SC 29634, USA; eshrews@g.clemson.edu (E.D.W.); kjoseph@clemson.edu (J.W.K.)
2 X-ray Science Division, Advanced Photon Source, Argonne National Laboratory, Lemont, IL 60439, USA; ktaddei@anl.gov
3 Division of Science, Mathematics and Technology, Governors State University, University Park, IL 60484-0975, USA; kranmohotti@govst.edu
4 University of Missouri Research Reactor (MURR), University of Missouri, Columbia, MO 65211, USA; nnydg@missouri.edu (N.N.); heitmannt@missouri.edu (T.H.)
5 Department of Physics and Astronomy, University of Missouri, Columbia, MO 65211, USA
6 Department of Chemistry, University of Missouri, Columbia, MO 65211, USA
* Correspondence: sanjeewal@missouri.edu

Abstract: Novel quantum materials offer the opportunity to expand next-generation computers, high-precision sensors, and new energy technologies. Among the most important factors influencing the development of quantum materials research is the ability of inorganic and materials chemists to grow high-quality single crystals. Here, the synthesis, structure characterization and magnetic properties of $Na_2Cu_3(SeO_3)_4$ are reported. It exhibits a novel two-dimensional (2D) structure with isolated layers of Cu nets. Single crystals of $Na_2Cu_3(SeO_3)_4$ were grown using a low-temperature hydrothermal method. Single-crystal X-ray diffraction reveals that $Na_2Cu_3(SeO_3)_4$ crystallizes in the monoclinic crystal system and has space group symmetry of $P2_1/n$ (No.14) with a unit cell of a = 8.1704(4) Å, b = 5.1659(2) Å, c = 14.7406(6) Å, β = 100.86(2), V = 611.01(5) Å^3 and Z = 2. $Na_2Cu_3(SeO_3)_4$ comprises a 2D Cu-O-Cu lattice containing two unique copper sites, a CuO_6 octahedra and a CuO_5 square pyramid. The SeO_3 groups bridge the 2D Cu-O-Cu layers isolating the neighboring Cu-O-Cu layers, thereby enhancing their 2D nature. Magnetic properties were determined by measuring the magnetic susceptibility of an array of randomly oriented single crystals of $Na_2Cu_3(SeO_3)_4$. The temperature-dependent magnetic measurement shows an antiferromagnetic transition at T_N = 4 K. These results suggest the fruitfulness of hydrothermal synthesis in achieving novel quantum materials and encourage future work on the chemistry of transition metal selenite.

Keywords: hydrothermal synthesis; crystal structure; copper(II); antiferromagnetism; two-dimensional structure

Citation: Williams, E.D.; Taddei, K.M.; Ranmohotti, K.G.S.; Narayanan, N.; Heitmann, T.; Kolis, J.W.; Sanjeewa, L.D. Coexistence of Long-Range Magnetic Order and Magnetic Frustration of a Novel Two-Dimensional $S = 1/2$ Structure: $Na_2Cu_3(SeO_3)_4$. *Magnetism* **2024**, *4*, 35–46. https://doi.org/10.3390/magnetism4010003

Academic Editor: Da Li

Received: 1 November 2023
Revised: 30 January 2024
Accepted: 2 February 2024
Published: 13 February 2024

1. Introduction

The pursuit of quantum materials (QMs) is driven both by a fundamental interest in their exotic physics and by the imminent practicality of their emergent properties, which may usher in a new era of quantum device designs [1–3]. The scientific interest is largely driven by the potential to isolate new forms of matter that are predicted to host novel physical properties among the nonclassical phases, including those of quantum spin liquids (QSLs), emergent topological states, spin–orbit coupled metals, Dirac semi-metals, Weyl semi-metals, topological Mott insulators, and topological axion insulators [3–6]. One of the most important factors influencing the development of quantum materials research is that

of the ability of inorganic and materials chemists to grow high-quality single crystals [3]. However, attempts to synthesize and design novel quantum materials merely through thermally coupling the target ingredients has proven to be somewhat difficult. Therefore, as materials chemists, our target is to develop new synthetic tools to grow high-quality bulk single crystals composed of novel quantum materials [7–9].

Over the last decades, two-dimensional (2D) magnetic materials with the spin state of $S = 1/2$ have gained attention as one such class of materials since they can exhibit exotic quantum properties such as that of the quantum spin liquid state [10]. The combination of an $S = 1/2$ center and the confinement of a 2D lattice highly enhances the potential for exotic magnetic states by creating strong magnetic frustration that can prevent a long-range magnetic order. Quantum fluctuations can arise through specific 2D lattice arrangements of the magnetic ions that, due to their geometry, prevent the simultaneous satisfaction of all the local antiferromagnetic magnetic interactions, thereby leading to massively degenerate ground states (geometric frustration). Common examples of such lattices are those of 2D triangular and Kagome magnetic lattices. At the other end of the spectrum are 2D honeycomb magnetic lattices. In honeycomb magnetic lattices, the magnetic frustration arises from competing interactions rather than geometric constraints [11,12]. This provides an alternate route to a quantum spin liquid state through the well-known resonating valence state proposed by Anderson as a potential explanation for high-temperature superconductivity [11]. Therefore, our main interest is to find 2D magnetic lattices built of $S = 1/2$ ions to enhance the quantum fluctuation and perform detailed theoretical and experimental investigations of their physical properties [11–14].

One approach that has proven fruitful recently is to synthesize novel 2D quantum materials using the high-pressure hydrothermal synthesis method [15]. Hydrothermal synthesis offers a powerful and promising strategy of controlling the structures and of thus controlling the corresponding desired properties. Hydrothermal synthesis can be performed in two different methods. One of these uses well-known, commercially available metal autoclaves ("digestion vessels") that are lined with inert fluoropolymers. These autoclaves are simple and convenient to use and can easily contain solutions that are acidic, basic or strongly oxidizing. However, the primary limitation to these autoclaves is their temperature limit since the fluoropolymer starts to melt at $T > 245$ °C. The second method employs high-pressure synthesis that can be performed at temperatures well above 245 °C using the Inconel 718 Tuttle cold-seal autoclave, which can stand an internal pressure of 1–3 kbar and temperatures of up to 700 °C [15]. This method has been very successful in growing larger crystals of both transition metal-based and rare earth-based oxide materials. Moreover, the high-temperature (T ~700 °C) hydrothermal technique also has the capability of producing larger single crystals that can be used for neutron scattering studies that allow us to determine many of the details of the magnetic behavior of the target materials. Our group has extensively used both of these methods to grow novel magnetic materials [16–19].

The hydrothermal synthesis of transition metal-based oxyanions has huge potential for making novel materials since the pressure (external stimulus) can stabilize the metastable phases that cannot be otherwise achieved by using traditional solid-state synthesis [16–19]. Moreover, many oxyanion tetrahedra are stable and magnetically silent, and they display an enormous range of chemical bonding modes [20,21]. Therefore, many different structures can be achieved. We successfully employed the hydrothermal method to synthesize numerous first-row transition metal structures with $[VO_4]^{3-}$, $[MoO_4]^{2-}$, $[AsO_4]^{3-}$ and $[GeO_4]^{4-}$ compounds using the high-temperature hydrothermal method [22–25]. Recently we undertook a project to explore the magnetism of transition metal-based selenium(IV) structures [26,27]. Although a wide range of metal selenites have been reported, [28,29] the investigation of the magnetic properties of transition metal selenium(IV) oxyanions has been very limited, and only a handful of reports are available in the literature. Furthermore, selenium can adapt $[SeO_3]^{2-}$ and $[Se_2O_5]^{2-}$ oxyanion configurations, which can form a high number of different structural arrangements in extended solid structures providing a rich and diverse crystal chemistry [30–32].

Therefore, we now extend our hydrothermal synthesis to explore selenite (SeO_3^{2-})-based transition metal compounds and perform detailed physical property characterizations and magnetic structure determinations using neutron diffraction in order to search for novel magnetic ground states. The $[SeO_3]^{2-}$ group has an active lone pair, which can give rise to acentric crystal structures with interesting magnetic properties such as skyrmions [33]. The compounds of $TM_3(SeO_3)_3$ H_2O (*TM* = Mn, Co, Ni) and $Na_2Co_3(SeO_3)_2(OH)$ are two recent examples where we performed comprehensive magnetic and neutron diffraction studies [26,27]. $TM_3(SeO_3)_3$ H_2O (*TM* = Mn, Co, Ni) structures are three-dimensional (3D) bulk materials with low-dimensional magnetic lattices and behave like low-dimensional systems as well. The compound of $Na_2Co_3(SeO_3)_2(OH)$ is an overall two-dimensional structure with a one-dimensional (1D) Co-O-Co sawtooth magnetic lattice. Recently, Zhong et al. and Liu et al. reported the hydrothermal synthesis and detailed physical property characterizations of two new cobalt(II) selenites, which were $Co_2SeO_3(OH)_2$ and $BaCo_2(SeO_3)_3$ 3H2O, respectively [34,35]. Both of these compounds comprised bulk 3D crystal structures with interesting magnetic properties. The $K_2M(SeO_3)_2$, *M* = Co, Ni series is another interesting addition to the transition metal-based selenite compounds [36,37]. These compounds have a perfect 2D triangular magnetic lattice and display strongly frustrated magnetism. In 2020, Zhong et al. also reported another cobalt(II) selenite, namely that of $K_2Co_2(SeO_3)_3$, which comprises Co^{2+}-dimers made from a face-sharing CoO_6 octahedra [38]. These dimers are arranged in a 2D geometrically frustrated triangular lattice. In this system, no long-range magnetic ordering was observed down to 0.35 K, thereby suggesting that the system is magnetically frustrated. It is thus of interest to synthesize and study the physical properties of new transition metal-based selenite structures to search for low-dimensional, magnetically frustrated systems.

In this paper, we report the hydrothermal synthesis of $Na_2Cu_3(SeO_3)_4$ single crystals using the mild hydrothermal method. The new $Na_2Cu_3(SeO_3)_4$ structure contains a 2D Cu-O-Cu lattice made from edge-shared CuO_6 and CuO_5 polyhedra. The SeO_3 groups separate the layers in this 2D Cu-O-Cu lattice by reducing the dimensionality of the structure with the non-magnetic Na ions occupying the space between the Cu-O-Se layers. The magnetic properties of the system were studied using multiple experimental methods including magnetic susceptibility and isothermal magnetization. Magnetic susceptibility measurements reveal the presence of an antiferromagnetic transition at T_N = 4 K, and the $Na_2Cu_3(SeO_3)_4$ compound exhibits a novel 2D spin lattice with exciting magnetic properties.

2. Experimental Section

2.1. Hydrothermal Synthesis of $Na_2Cu_3(SeO_3)_4$

The synthesis of $Na_2Cu_3(SeO_3)_4$ was carried out using a hydrothermal method at low temperatures. A typical reaction was performed using the 2:3:4 stoichiometric ratio of $NaHCO_3$ (Thermo Scientific Chemicals, 99.7%), $Cu(CH_3COO)_2$ (Thermo Scientific Chemicals, 99%) and SeO_2 (Thermo Scientific Chemicals, 99.8%). A 0.8 g mixture of reactants was loaded into a Teflon-lined stainless steel autoclave, which was then well-sealed with 8 mL of de-ionized water. The reaction mixture was heated at 220 °C for 14 days. After the reaction, columnar green crystals (1 mm, Figure 1) were recovered using suction filtration by washing them with de-ionized water and acetone. The final product of the reaction contained equal amounts of $CuSeO_3$ $2H_2O$ (blue column crystals) and $Na_2Cu_3(SeO_3)_4$. All attempts to make the pure phase of $Na_2Cu_3(SeO_3)_4$ using different stoichiometric ratios were unsuccessful.

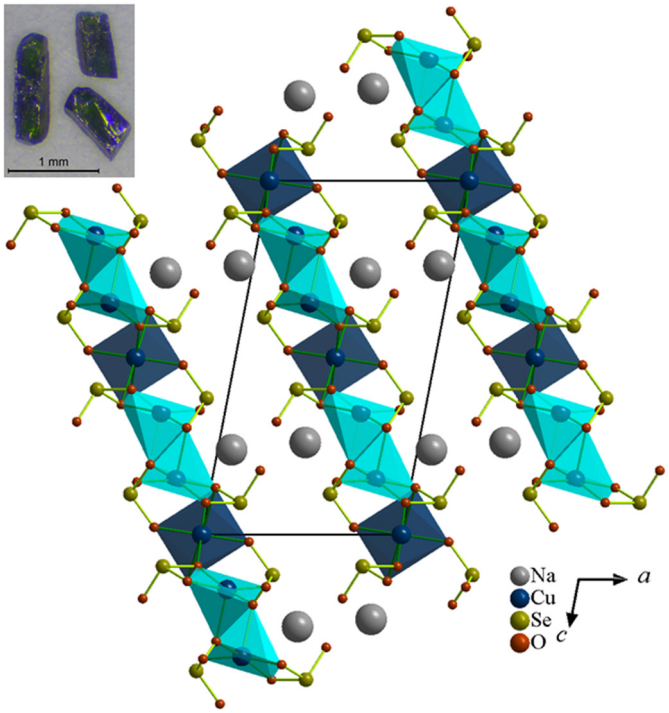

Figure 1. Partial polyhedral view of $Na_2Cu_3(SeO_3)_4$ projected along the *b*-axis showing packing of Cu-O-Se 2D layers. The Na ions reside between the Cu-O-Se layers. Hydrothermally grown single crystals of $Na_2Cu_3(SeO_3)_4$ are shown on the top left-hand corner.

2.2. Single-Crystal X-ray Diffraction

Before determining the single-crystal structure of $Na_2Cu_3(SeO_3)_4$, single crystals were sonicated in water and acetone to remove any surface impurities. The SXRD was performed using a Bruker Quest D8 single-crystal X-ray diffractometer. The data were collected at room temperature utilizing Mo Kα radiation, λ = 0.71073 Å. The crystal diffraction images were collected using ϕ and ω scans. The diffractometer was equipped with an Incoatec IμS source using the APEX3 software suite for data setup, collection and processing [39]. The structure was resolved using intrinsic phasing and full-matrix least-square methods with refinement on F^2. Structure refinements were performed using the SHELXTL software suite [40]. All atoms were first refined with isotropic displacement parameters, which were then converted to anisotropic displacement parameters and allowed to refine. Additionally, energy-dispersive spectroscopy analysis (EDS) was performed using a Hitachi S-3400 scanning electron microscope equipped with an OXFORD EDX microprobe to confirm the elemental composition of single-crystal samples. The unit cell parameters and selected bond distances and angles of $Na_2Cu_3(SeO_3)_4$ are displayed in Tables 1 and 2, respectively. The fractional atomic coordinates and equivalent isotropic displacement parameters are shown in Table 3.

Table 1. Crystallographic data of $Na_2Cu_3(SeO_3)_4$ determined through single-crystal X-ray diffraction.

Empirical Formula	**$Na_2Cu_3(SeO_3)_4$**
formula weight (g/mol)	744.44
crystal system	monoclinic
crystal dimensions, mm	0.02 × 0.02 × 0.02
space group, *Z*	$P2_1/n$ (no.14), 2

Table 1. *Cont.*

Empirical Formula	**$Na_2Cu_3(SeO_3)_4$**
T, K	298
a, Å	8.1704(4)
b, Å	5.1659(2)
c, Å	14.7406(6)
β, °	100.86(2)
volume, Å^3	611.01(5)
D(calc), g/cm^3)	4.046
μ (Mo Kα), mm^{-1}	17.218
F(000)	682
Tmax, Tmin	1.0000, 0.6887
2θ range	2.66-30.48
reflections collected	25336
data/restraints/parameters	1866/0/97
final R [$I > 2\sigma(I)$] R_1, R_{w2}	0.0216, 0.0525
final R (all data) R_1, R_{w2}	0.0295, 0.0525
GoF	1.023
largest diff. peak/hole, e/Å^3	1.216/−0.939

Table 2. Selected bond distances (Å) and angles (°) of $Na_2Cu_3(SeO_3)_4$.

	$Cu(1)O_6$	$Cu(2)O_5$	
Cu(1)-O(1) × 2	1.956(2)	Cu(2)-O(1)	2.002(2)
Cu(1)-O(2) × 2	1.971(2)	Cu(2)-O(3)	1.963(2)
Cu(1)-O(3) × 2	2.436(2)	Cu(2)-O(4)	1.994(2)
		Cu(2)-O(4)	2.392(2)
		Cu(2)-O(5)	1.924(2)
$Se(1)O_3$		$Se(2)O_3$	
Se(1)-O(2)	1.682(2)	Se(2)-O(1)	1.642(2)
Se(1)-O(4)	1.722(2)	Se(2)-O(3)	1.726(2)
Se(1)-O(5)	1.686(2)	Se(2)-O(6)	1.760(2)
Cu(1)-O(1)-Cu(2)	137.3(2)	Cu(1)···Cu(2)	3.476(2)
Cu(1)-O(3)-Cu(2)	103.9(1)	Cu(1)···Cu(2)	3.686(2)
Cu(2)-O(4)-Cu(2)	120.7(3)	Cu(2)···Cu(2)	3.816(2)

Table 3. Fractional atomic coordinates and isotropic or equivalent isotropic displacement parameters ($Å^2$) of $Na_2Cu_3(SeO_3)_4$.

Atom	*Wyckoff*	*x*	*y*	*z*	*Ueq*
Na(1)	4*e*	0.9306(2)	0.5284(5)	0.2397(3)	0.01690(3)
Cu(1)	2*c*	0.5000	0	0.5000	0.01027(5)
Cu(2)	4*e*	0.3191(2)	0.5281(1)	0.3447(3)	0.00971(3)
Se(1)	4*e*	0.1053(5)	0.0115(3)	0.3856(3)	0.01148(4)
Se(2)	4*e*	0.6623(6)	0.4853(2)	0.4101(3)	0.01176(6)
O(1)	4*e*	0.4902(3)	0.2805(2)	0.4100(3)	0.01192(2)
O(2)	4*e*	0.2555(7)	−0.0353(4)	0.4790(5)	0.02284(5)
O(3)	4*e*	0.5260(6)	0.7310(5)	0.3677(5)	0.01101(3)
O(4)	4*e*	0.1762(1)	−0.1664(2)	0.3019(2)	0.01294(3)
O(5)	4*e*	0.1268(2)	0.3197(2)	0.3518(3)	0.01166(3)
O(6)	4*e*	0.7326(5)	0.3840(5)	0.3190(5)	0.02812(4)

2.3. Magnetic Property Characterization

A quantum design magnetic property measurement system (MPMS) was used to measure temperature- and field-dependent magnetic susceptibility. Here, single crystals of $Na_2Cu_3(SeO_4)_4$ were randomly packed using GE varnish. The temperature-dependent magnetization measurements were carried out using 16.5 mg of crystals from 2 to 350 K in an applied magnetic field of up to 50 kOe. Additionally, magnetization data were collected in both zero-field-cooled (ZFC) and field-cooled (FC) modes in an applied field of 10 kOe. The ZFC measurement was performed by cooling the sample from 350 K to 2 K without applying any external field. Upon reaching 2 K, a 10 kOe magnetic field was applied, and magnetization was measured while warming to 350 K. For the FC measurement, the sample was cooled from 350 K to 2 K in an applied magnetic field of 10 kOe while collecting magnetization data. The isothermal magnetization measurements were performed between 2 and 100 K up to a 60 kOe magnetic field.

3. Results and Discussion

3.1. Synthesis and Crystal Structure of $Na_2Cu_3(SeO_3)_4$

The synthetic approach to $Na_2Cu_3(SeO_3)_4$ single crystals was drawn from recent the synthesis of other transition metal selenites possessing low-dimensional structural features. In general, synthesis was performed using the readily available soluble transition metal halides, acetates and selenium(IV) oxide. In addition, an alkali carbonate or bicarbonate was used in the reaction because they can sometimes be the primary structural building block between the transition metal selenite layers or chains. In the present study, water was used as the mineralizer/reaction medium. Two major products were observed in the reaction, namely $CuSeO_3$ $2H_2O$ and $Na_2Cu_3(SeO_3)_4$. The $CuSeO_3$ $2H_2O$ structure was reported previously with some preliminary magnetic measurements [41]. The $Na_2Cu_3(SeO_3)_4$ is a new addition to the collection of transition metal selenite structures. Additional synthetic work was performed using different chemical sources of copper and different stoichiometric ratios to achieve the phase-pure reaction of $Na_2Cu_3(SeO_3)_4$, but all these reactions formed either unidentified polycrystalline phases or $CuSeO_3$ $2H_2O$ single crystals [41]. In most of these cases, $CuSeO_3$ $2H_2O$ forms larger single crystals that are 2–5 mm. Thus, growing larger single crystals or the pure powder phase of $Na_2Cu_3(SeO_3)_4$ was unsuccessful, which unfortunately currently prevents magnetic structure characterization using neutron scattering.

The single-crystal structures were characterized using the SXRD measurements at room temperature. The $Na_2Cu_3(SeO_3)_4$ structure represents a new structure type with

unique 2D layers, which crystalizes in a monoclinic crystal system, with a $P2_1/n$ (No.14) space group with the unit cell parameters of a = 8.1704(4) Å, b = 5.1659(2) Å, c = 14.7406(6) Å, β = 100.86(2), V = 611.01(5) Å3 and Z = 2, as depicted in Table 1. To understand its magnetic behavior, it is important to understand its structural aspects in some detail. The structure comprises one unique Na (4*e*), two Cu (4*e* and 2*c*), two Se (4*e*) and six oxygen atoms (4*e*), as shown in Table 3. As depicted in Figure 1, $Na_2Cu_3(SeO_3)_4$ forms a 2D structure that is made from CuO_n (n = 5, 6) polyhedra and SeO_3 units. The sodium ions occupy the gaps between the Cu-O-Se layers, while the two Cu sites form two different polyhedra, $Cu(1)O_6$ octahedra and a $Cu(2)O_5$ square pyramid, respectively. Figure 2a displays the connectivity between the $Cu(1)O_6$ octahedra and $Cu(2)O_5$ square pyramid (shown in two different colors for clarity) on the *ac*-plane where they form 2D layers of Cu-O-Cu. The connectivity between the $Cu(1)O_6$ and $Cu(2)O_5$ units can be simplified as forming 1D chains along the [111] direction. Within the chains, two $Cu(2)O_5$ units connect through O(2) forming dimers, and each dimer is connected with two $Cu(1)O_6$ octahedra on opposite sides of the dimer. The Cu(1) and Cu(2) octahedra then form a 2D lattice made from squares of Cu centers where each square is made from two Cu(1) and two Cu(2) centers, as shown in Figure 2b.

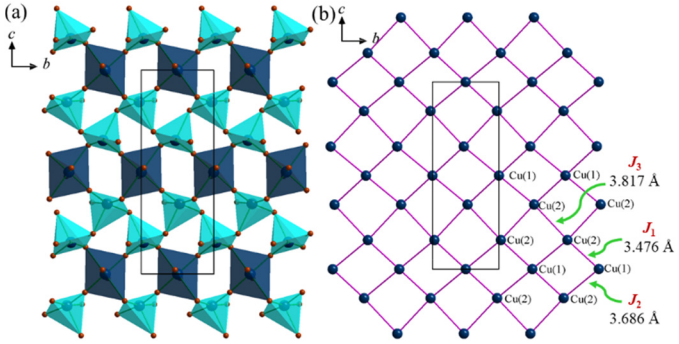

Figure 2. (**a**) Partial polyhedral view of the 2D Cu-O-Cu magnetic lattice on the *bc*-plane. (**b**) Nearest neighbor interactions between the Cu(1) and Cu(2) centers. The unequal J_1, J_2 and J_3 exchange interactions are shown using a solid pink line. The Cu(1)–Cu(2), J_1; Cu(1)–Cu(2), J_2; and Cu(2)–Cu(2), J_3 distances are 3.476, 3.686 and 3.817 Å, respectively.

Figure 3a shows the local connectivity of $Cu(1)O_6$ with $Cu(2)O_5$ units. As shown in Figure 3a, each $Cu(1)O_6$ unit is connected with four $Cu(1)O_5$ units through two equatorial oxygens, O(1), and two axial oxygens, O(3). Each $Cu(2)O_5$ unit is connected with two additional $Cu(2)O_5$ units and two $Cu(1)O_6$ units, as shown in Figure 3b. It is interesting to note that the apex oxygen, O(4), of one $Cu(2)O_5$ square pyramid is connected with the base of another $Cu(2)O_5$ square pyramid creating a Cu(2)-O-Cu(2) chain along the *b*-axis, as shown in Figure 3b. The 2D Cu-O-Cu layers are decorated by the $[SeO_3]$ groups in each side of the layer. The apical $Se(1)O_3$ group is connected with one $Cu(1)O_6$ unit and three $Cu(1)O_5$ units, while the $Se(2)O_3$ group connects with two $Cu(1)O_6$ units and one $Cu(2)O_5$ unit, as shown in Figure 3c,d.

The bond distances and angles of the $Na_2Cu_3(SeO_3)_4$ structure are of interest in the unique 2D structure. The Cu-O bond distances of $Cu(1)O_6$ range from 1.956(2) to 2.436(2) Å, thereby adopting a highly distorted CuO_6 octahedron. Similarly, the $Cu(2)O_5$ units are also have a highly distorted nature, with Cu-O bond lengths ranging from 1.924(2) to 2.392(2) Å. The average Cu-O bond lengths of CuO_6 and CuO_5 are 2.121 and 2.055 Å, respectively. These average bond distances agree well with the sum of the Shannon crystal radii for six coordinated $Cu^{2+}O_6$ (2.13 Å) units and five coordinated $Cu^{2+}O_5$ (2.05 Å) units, respectively [40]. The average Se(1)-O and Se(2)-O distances are 1.696 and 1.709 Å, respectively, which are comparable with the Shannon crystal radii for three coordinated $Se^{+4}O_3$ (1.86 Å) units [40]. Since each $Cu(1)O_6$ unit is surrounded by four $Cu(2)O_5$ units (Figure 2), Cu(1) has the four nearest neighbor Cu(2) atoms. Since Cu(1) and Cu(2) connect through different oxygen atoms, two different exchange parameters are created, J_1 (3.476 Å)

and J_2 (3.686 Å), as highlighted in Figure 2b. Additionally, Cu(2) forms dimers with the Cu(2)−Cu(2) distances of 3.817 Å, J_3. The corner-sharing bond angles between $Cu(1)O_6$ and $Cu(2)O_5$ are 137.3(2) and 103.9(1)° for Cu(1)−O(1)−Cu(2) and Cu(1)−O(3)−Cu(2), respectively. The corner-sharing bond between the $Cu(2)O_5$ in the dimer, Cu(2)-O(4)-Cu(2), is 120.7(3)°. This wide variety of bond distances and angles is due to the lower symmetry of the structure. Additionally, the presence of different CuO_5 and CuO_6 geometries in $Na_2Cu_3(SeO_3)_4$ introduces additional variables. Given the diversity of bond distances, angles and multiple superexchange pathways of the $Na_2Cu_3(SeO_3)_4$ structure, complex magnetic interactions can be expected. In this way, the $Na_2Cu_3(SeO_3)_4$ structure is fairly complex, even though it has a simple 2D Cu magnetic lattice.

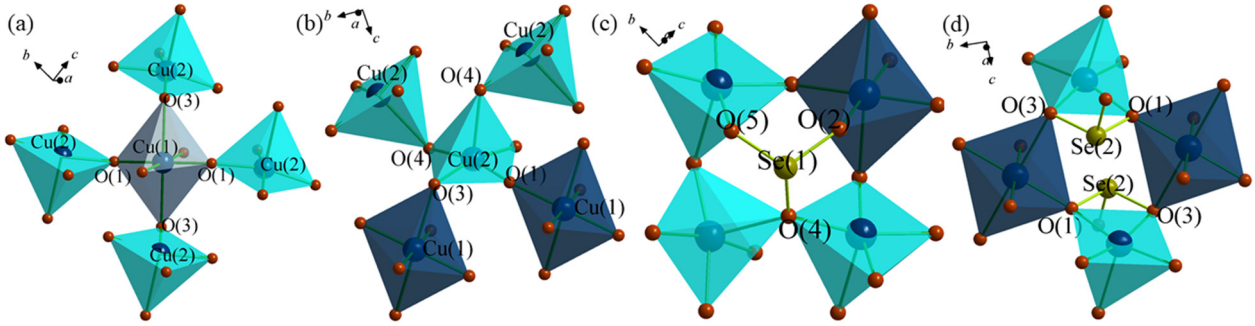

Figure 3. (**a**) Connectivity between the $Cu(1)O_6$ and $Cu(2)O_5$ units. (**b**) Connectivity between the $Cu(2)O_5$ and $Cu(1)O_6$ units. (**c**) Connectivity between the $Cu(1)O_6$, $Cu(2)O_5$ and $Se(1)O_3$ units. (**d**) Connectivity between the $Cu(1)O_6$, $Cu(2)O_5$ and $Se(2)O_3$ units.

3.2. Magnetic Properties of $Na_2Cu_3(SeO_3)_4$

The temperature-dependent magnetization of $\chi = M/H$ of $Na_2Cu_3(SeO_3)_4$ was measured using a collection of single crystals arranged in random orientations. The magnetic susceptibility data were collected in the form of FC and ZFC modes between 2 and 350 K, and the FC-ZFC curves exhibited the same magnetic behavior. Figure 4a displays the magnetic susceptibility and inverse magnetic susceptibility with an applied field of 10 kOe. The magnetic susceptibility curve at 10 kOe exhibits a sharp upturn at lower temperature potentially, thereby indicating ferromagnetic-type behavior (Figure 4a). However, at a lower field of $H < 10$ kOe, the magnetic susceptibility displayed a peak at 4 K, likely indicating long-range antiferromagnetic behavior with $T_N = 4$ K. The Curie–Weiss fit was performed in the temperature range of 150–350 K and resulted in $\theta_{CW} = -196$ K and the effective magnetic moment of 2.18 μ_B/Cu. The effective magnetic moment was slightly higher than the ideal spin-only moment of Cu^{2+} ($S = 1/2$) being 1.73 μ_B. This may be due to the orbital contribution of Cu^{2+} in the distorted CuO_6 and CuO_5 environment. Similar higher values have been observed in 2D Cu magnetic systems such as $BaAg_2Cu(VO_4)_2$, $Cu_5(VO_4)_2(OH)_4$ and $Cu_5O_2(SeO_3)_2Cl_2$ [42–45]. The negative and unusually large θ_{CW} indicates the strong antiferromagnetic interactions between the Cu centers within the 2D magnetic lattice. The empirical magnetic frustration was calculated using $f = |\theta_{CW}|/T_N \sim 54$, which supports the strong magnetic frustration in the $Na_2Cu_3(SeO_3)_4$ magnetic lattice. Similar high values have been observed for other copper complexes such as $Cu_{13}(VO_4)_4(OH)_{10}F_4$ ($f = 21$), $Cu_5O_2(SeO_3)_2Cl_2$ ($f = 7$) and $Cu_5V_2O_{10}$ ($f = 13$). Strong frustration is considered to be present in materials with $f > 10$. The magnetic frustration of $Na_2Cu_3(SeO_3)_4$ may occur as a result of competitive interactions between crystallographically distinct Cu sites within the 2D magnetic lattice, as exemplified in Figure 2b. However, in order to confirm the origin of the magnetic frustration of $Na_2Cu_3(SeO_3)_4$, detailed theoretical and inelastic neutron scattering studies will be necessary. A detailed theoretical investigation has been performed on frustrated the square-lattice antiferromagnets of Ba_2CuTeO_6 and Ba_2CuWO_6. Magnetic frustration in these compounds results from the competition between the nearest-neighbor interaction, J_1, and the next-nearest-neighbor interaction, J_2, and a quantum spin liquid

state is predicted for $J_2/J_1 = 0.5$ [45–49]. It is noteworthy to mention that $Cu_5V_2O_{10}$ exhibits an unusually high effective magnetic moment (2.49 μ_B) and that $\theta_{CW} = -263$ K with the frustration index being around $f = 13$. Moreover, $Cu_5V_2O_{10}$ also possesses zigzag chains that are made from highly distorted CuO_6 octahedra and CuO_5 trigonal bipyramids. One of the most remarkable features of both $Cu_5V_2O_{10}$ and $Na_2Cu_3(SeO_3)_4$ is that they consist of Cu squares made from copper ions through the cross-connection between the CuO_6 and CuO_5 units. The magnetic properties of $Cu_5V_2O_{10}$ are highly anisotropic, and we expect that $Na_2Cu_3(SeO_3)_4$ could be the same. Figure 4b shows the temperature dependence of the magnetic susceptibility to be below 15 K when collected under various magnetic fields of $H = 0.1$–50 kOe. At 0.1 and 0.5 kOe, the magnetic susceptibility exhibits a sharp peak at around 4 K. At 1 kOe, the peak becomes broader and moves to a lower temperature. A further increase in the magnetic field pushes the transition to a lower temperature while also suppressing the clear downturn suggesting a gradual development of a ferromagnetic/ferrimagnetic phase. This behavior was also observed for the isothermal magnetization data. Figure 4c shows the isothermal magnetization data collected across tthe temperatures of 2–50 K. At 2 K, the isothermal magnetization exhibits a rapid increase with the applied field and reaches saturation at a relatively lower magnetic field of $H = 10$ kOe. The isothermal magnetization at 2 K reaches a saturation value of 0.3 μ_B/Cu at 10 kOe. This is much smaller compared with the full moment of Cu^{2+} with $S = 1/2$. This type of behavior was also observed for $Cu_5(VO_4)_2(OH)_4$, which was explained as a 1/5 magnetization plateau [44]. Above T_N, the magnetization follows a curvature behavior, which confirms the establishment of the ferromagnetic-like phase at higher fields. Similar *M-H* behavior has also been reported for $Cu_5(VO_4)_2(OH)_4$ and $BaAg_2Cu(VO_4)_2$, which suggests that these structures behave like antiferromagnets at lower fields but that sufficiently high magnetic fields can stabilize the ferromagnetic phase above the T_N [50,51]. Specific heat measurements under different applied magnetic fields would further confirm this exotic behavior.

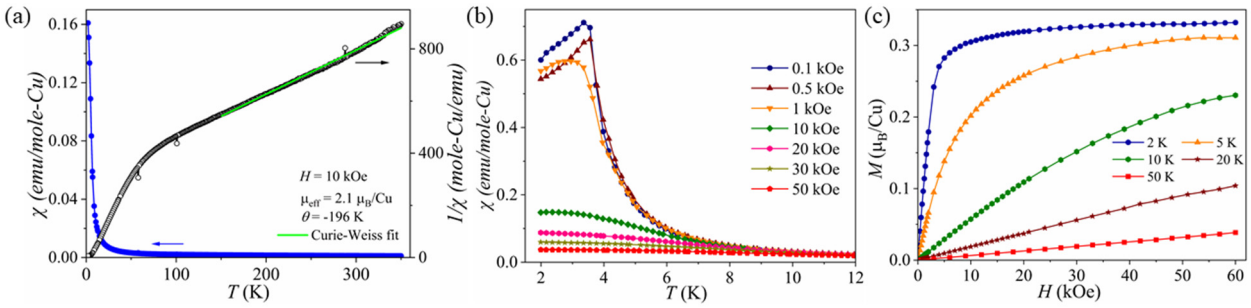

Figure 4. (**a**) Magnetic susceptibility, χ, and inverse magnetic susceptibility, 1/χ, as a function of temperature, *T*, measured using the randomly oriented single-crystal sample of $Na_2Cu_3(SeO_3)_4$ measured at $H = 10$ kOe. (**b**) Magnetization curves of $Na_2Cu_3(SeO_3)_4$ measured in different magnetic fields ($H = 0.1$–50 kOe) below 15 K. (**c**) Isothermal magnetization data obtained at 2–50 K up to 60 kOe.

4. Conclusions

Low-spin 2D magnetic lattices have attracted considerable interest since they are often predicted and shown to exhibit complex magnetic behavior. The combination of a transition metal magnetic lattice with the SeO_3 oxyanion group as a bridging unit provides a rich field of study in this regard and allows for significant tunability both to the structure and to the magnetic ion. In this study, we report the synthesis and magnetic data of a new material with an unusual 2D Cu^{2+} ($S = ½$) magnetic lattice, namely that of $Na_2Cu_3(SeO_3)_4$, which is made from two unique CuO_6 and CuO_5 units. Due to the presence of two different geometries of Cu–O polyhedra in the magnetic lattice, multiple nearest-neighbor interactions are expected. The preliminary magnetic properties were examined using a randomly oriented single-crystal sample, which reveal an antiferromagnetic transition at $T_N = 4$ K. However, isothermal magnetization data suggested that at a lower applied

field $Na_2Cu_3(SeO_3)_4$ becomes ferromagnetic. In addition, a very high $f = |\theta_{CW}|/T_N \sim 54$ value suggests significant magnetic frustration. The high degree of frustration in the 2D $S = 1/2$ material along with the complex field dependence of the magnetic behavior implies that an unusual magnetic structure exists in this new material. Our work highlights the complexity of structure formation between the Cu^{2+} magnetic ions and the SeO_3 groups. Future anisotropic magnetic measurements, neutron diffraction and theoretical study will elucidate the detailed magnetism of this novel 2D $Na_2Cu_3(SeO_3)_4$. We hope our work will inspire the further synthetic, structural and magnetic studies of the transition metal-based selenite compounds.

Author Contributions: Formal analysis, K.G.S.R.; funding acquisition, J.W.K.; methodology, E.D.W.; writing—original draft, N.N. and L.D.S.; writing—review and editing, K.M.T. and T.H. All authors have read and agreed to the published version of the manuscript.

Funding: This work was supported in part by a University of Missouri Research Council Grant (grant number: URC-22-021). The work at University of Missouri and Clemson University was supported by awards from the NSF DMR—2219129.

Data Availability Statement: CCDC 2304244 contain the supporting crystallographic data for this paper. These data can be obtained free of charge through www.ccdc.cam.ac.uk/data_request/cif (28 October 2023), by emailing data_request@ccdc.cam.ac.uk or by contacting The Cambridge Crystallographic Data Centre, 12 Union Road, Cambridge, CB2 1EZ, UK, fax: +44-1223-336033.

Acknowledgments: This research used resources at the Missouri University Research Reactor (MURR).

Conflicts of Interest: The authors declare no conflicts of interest.

References

1. Tokura, Y.; Kawasaki, M.; Nagaosa, N. Emergent Functions of Quantum Materials. *Nat. Phys.* **2017**, *13*, 1056–1068. [CrossRef]
2. Keimer, B.; Moore, J. The Physics of Quantum Materials. *Nat. Phys.* **2017**, *13*, 1045–1055. [CrossRef]
3. Giustino, F.; Lee, J.H.; Trier, F.; Bibes, M.; Winter, S.M.; Valentí, R.; Son, Y.; Taillefer, L.; Heil, C.; Figueroa, A.I.; et al. The 2021 Quantum Materials Roadmap. *J. Phys. Mater.* **2020**, *3*, 042006. [CrossRef]
4. Balents, L. Spin Liquids in Frustrated Magnets. *Nature* **2010**, *464*, 199–208. [CrossRef]
5. Head-Marsden, K.; Flick, J.; Ciccarino, C.J.; Narang, P. Quantum Information and Algorithms for Correlated Quantum. *Chem. Rev.* **2021**, *121*, 3061–3120. [CrossRef]
6. Ni, X.; Yves, S.; Krasnok, A.; Alu, A. Topological Metamaterials. *Chem. Rev.* **2023**, *123*, 7585–7654. [CrossRef]
7. Wang, X.; Liu, X. High Pressure: A Feasible Tool for the Synthesis of Unprecedented Inorganic Compounds. *Inorg. Chem. Front.* **2020**, *7*, 2890–2898. [CrossRef]
8. Walsh, J.P.S.; Freedman, D.E. High-Pressure Synthesis: A New Frontier in the Search for Next-Generation Intermetallic Compounds. *Acc. Chem. Res.* **2018**, *51*, 1315–1323. [CrossRef]
9. Xiao, G.; Geng, T.; Zou, B. Emerging Functional Materials under High Pressure toward Enhanced Properties. *ACS Mater. Lett.* **2020**, *2*, 1233–1239. [CrossRef]
10. Knolle, J.; Moessner, R. A Field Guide to Spin Liquids. *Annu. Rev. Condens. Matter Phys.* **2019**, *10*, 451–472. [CrossRef]
11. Wen, J.; Yu, S.; Li, S.; Yu, W.; Li, J. Experimental Identification of Quantum Spin Liquids. *NPJ Quantum Mater.* **2019**, *4*, 12. [CrossRef]
12. Taddei, K.M.; Garlea, V.O.; Samarakoon, A.M.; Sanjeewa, L.D.; Xing, J.; Heitmann, T.W.; Cruz, C.; Sefat, A.S.; Parker, D. Zig-Zag Magnetic Order and Potential Kitaev Interactions in the Spin-1 Honeycomb Lattice $KNiAsO_4$. *Phys. Rev. Res.* **2023**, *5*, 013022. [CrossRef]
13. Xing, J.; Sanjeewa, L.D.; May, A.F.; Sefat, S.A. Synthesis and Anisotropic Magnetism in Quantum Spin Liquid Candidates $AYbSe_2$ (A = K and Rb). *APL Mater.* **2021**, *9*, 111104. [CrossRef]
14. Xie, T.; Eberharter, A.A.; Xing, J.; Nishimoto, S.; Brando, M.; Khanenko, P.; Sichelschmidt, J.; Turrini, A.A.; Mazzone, D.G.; Naumov, P.G.; et al. Complete field-induced spectral response of the spin-1/2 triangular-lattice antiferromagnet $CsYbSe_2$. *NPJ Quantum Mater.* **2023**, *8*, 48. [CrossRef]
15. McMillen, C.D.; Kolis, J.W. Hydrothermal Synthesis as a Route to Mineralogically-inspired Structures. *Dalton Trans.* **2016**, *45*, 2772–2784. [CrossRef]
16. Sanjeewa, L.D.; Garlea, V.O.; Fishman, R.S.; Foroughian, M.; Yin, L.; Xing, J.; Parker, D.S.; Pellizzeri, T.M.S.; Sefat, A.S.; Kolis, J.W. Field Tunable Magnetic Transitions of $CsCo_2(MoO_4)_2(OH)$: A Triangular Chain Structure with a Frustrated Geometry. *Mater. Chem. Front.* **2023**, *7*, 1058–1071. [CrossRef]

17. Sanjeewa, L.D.; Garlea, V.O.; McGuire, M.A.; Xing, J.; Cao, H.; Kolis, J.W.; Sefat, A.S. Observation of Large Magnetic Anisotropy and Field-induced Magnetic State in $SrCo(VO_4)(OH)$: A Structure with Quasi One-Dimensional Magnetic Chain. *Inorg. Chem.* **2020**, *59*, 1029–1037. [CrossRef]
18. Sanjeewa, L.D.; Ross, K.A.; Sarkis, C.L.; Nair, H.S.; McMillen, C.D.; Kolis, J.W. Single Crystals of Cubic Rare-Earth Pyrochlore Germanates: $RE_2Ge_2O_7$ (*RE* = Yb and Lu) Grown by a High-Temperature Hydrothermal Technique. *Inorg. Chem.* **2018**, *57*, 12456–12460. [CrossRef] [PubMed]
19. Matthew, P.; Sanjeewa, L.D.; McMillen, C.D.; Ross, K.A.; Sarkis, C.L.; Kolis, J.W. Hydrothermal Crystal Growth of Rare Earth Tin Cubic Pyrochlores, $RE_2Sn_2O_7$ (*RE* = La-Lu): Site Ordered, Low Defect Single Crystals. *Cryst. Growth Des.* **2019**, *19*, 4920–4926.
20. Krivovichev, S.V. Which Inorganic Structures are the Most Complex? *Angew. Chem. Int. Ed.* **2014**, *53*, 654–661. [CrossRef]
21. Bugaris, D.E.; zur Loye, H.-C. Materials Discovery by Flux Crystal Growth: Quaternary and Higher Order Oxides. *Angew. Chem. Int. Ed.* **2012**, *51*, 3780–3811. [CrossRef] [PubMed]
22. Liu, Y.; Sanjeewa, L.D.; Garlea, V.O.; Pellizzeri, T.M.S.; Kolis, J.W.; Sefat, A.S. Complex Magnetic Order in the Decorated Spin-chain System $Rb_2Mn_3(MoO_4)_3(OH)_2$. *Phys. Rev. B* **2020**, *101*, 064423. [CrossRef]
23. Garlea, V.O.; Sanjeewa, L.D.; McGuire, M.A.; Batista, C.D.; Samarakoon, A.M.; Graf, D.; Winn, B.; Ye, F.; Hoffmann, C.; Kolis, J.W. Exotic Magnetic Field-Induced Spin-Superstructures in a Mixed Honeycomb-Triangular Lattice System. *Phys. Rev. X* **2019**, *9*, 011038. [CrossRef]
24. Sanjeewa, L.D.; McGuire, M.A.; McMillen, C.D.; Garlea, V.O.; Kolis, J.W. Polar Materials with Isolated V^{4+} S = ½ Triangles: $NaSr_2V_3O_3(Ge_4O_{13})Cl$ and $KSr_2V_3O_3(Ge_4O_{13})Cl$. *Chem. Mater.* **2017**, *29*, 1404–1412. [CrossRef]
25. Garlea, O.; Sanjeewa, L.D.; McGuire, M.; Kumar, P.; Sulejmanovic, D.; He, J.; Hwu, S.-J. Complex Magnetic Behavior of the Sawtooth Fe Chains in $Rb_2Fe_2O(AsO_4)_2$. *Phys. Rev. B* **2014**, *89*, 014426. [CrossRef]
26. Sanjeewa, L.D.; Garlea, V.O.; Taddei, K.M.; Yin, L.; Xing, J.; Fishman, R.S.; Parker, D.S.; Sefat, S.A. $NaCo_2(SeO_3)_2(OH)$: Competing Magnetic Ground States of a New Sawtooth Structure with $3d^7$ Co^{2+} ions. *Inorg. Chem. Front.* **2022**, *9*, 4329–4340. [CrossRef]
27. Taddei, K.M.; Sanjeewa, L.D.; Xing, J.; Parker, D.; Podleznyak, A.; dela Cruz, C.; Sefat, A. Tunable Magnetic Order in Low-Symmetry SeO_3 Ligand Linked $TM_3(SeO_3)$ $3H_2O$ (*TM* = Mn, Co and Ni) Compounds. *Phys. Rev. M* **2020**, *4*, 024410. [CrossRef]
28. Menezes, L.T.; Gage, E.; Assoud, A.; Liang, M.; Halasyamani, P.S.; Kleinke, H. $Sr_6Ge_3OSe_{11}$: A Rationally Designed Noncentrosymmetric Oxyselenide with Polar $[GeOSe_3]$ Building Blocks. *Chem. Mater.* **2023**, *35*, 3033–3040. [CrossRef]
29. Liu, L.; Zhang, B.; Halasyamani, P.S.; Zhang, W. $Pb_2TiFO(SeO_3)_2Br$: A New Polar Compound with the Strongest Second Harmonic Generation in the Selenite Bromide Family. *J. Mater. Chem. C* **2021**, *9*, 6491–6497. [CrossRef]
30. Kovrugin, V.M.; Colmont, M.; Siidra, O.I.; Charkin, D.O.; Aliev, A.; Krivovichev, S.V.; Mentré, O. Synthesis and Structural Variety of First Mn and Bi Selenites and Selenite Chlorides. *Cryst. Mater.* **2019**, *234*, 141–153. [CrossRef]
31. Berdonosov, P.S.; Kuznetsova, E.S.; Dolgikh, V.A. Transition Metal Selenite Halides: A Fascinating Family of Magnetic Compounds. *Crystals* **2018**, *8*, 159. [CrossRef]
32. Choudhury, A.; Kumar, U.; Rao, C.N.R. Three-dimensional Organically Templated Open-Framework Transition Metal Selenites. *Angew. Chem. Int. Ed.* **2002**, *41*, 158–161. [CrossRef]
33. Qian, F.; Bannenberg, L.J.; Wilhelm, H.; Chaboussant, G.; Debeer-Schmitt, L.M.; Schmidt, M.P.; Aqee, A.; Palstra, T.T.M.; Brück, E.; Lefering, A.J.E.; et al. New Magnetic Phase of the Chiral Skyrmion Material Cu_2OSeO_3. *Sci. Adv.* **2018**, *4*, 7323.
34. Zhong, R.; Guo, S.; Ni, D.; Cava, R.J. Dicobalt (II) Hydroxo-selenite: Hydrothermal Synthesis, Crystal Structure and Magnetic Properties of $Co_2SeO_3(OH)_2$. *J. Solid State Chem.* **2020**, *285*, 121250. [CrossRef]
35. Liu, X.C.; Ouyang, C.W.; Xiao, T.T.; Cao, J.J.; Wang, J.X.; Xia, Z.C.; He, Z.Z.; Tong, W. Magnetism and ESR of the S_{eff} = 1/2 Antiferromagnet $BaCo_2(SeO_3)_3$ $3H_2O$ with Dimer-Chain Structure. *Phys. Rev. B* **2022**, *105*, 134417. [CrossRef]
36. Zhong, R.; Guo, S.; Cava, R.J. Frustrated magnetism in the layered triangular lattice materials $K_2Co(SeO_3)_2$ and $Rb_2Co(SeO_3)_2$. *Phys. Rev. B* **2020**, *4*, 084406. [CrossRef]
37. Li, Z.; Ouyang, Z.; Cao, J.; Liu, X.; Xiao, T.; Wang, L.; Liang, Y.; Tian, Z.; Wang, Z.; Xia, Z. $K_2Ni(SeO_3)_2$: A Perfect S = 1 Triangular-Lattice Antiferromagnet with Strong Geometric Frustration and Easy-Plane Anisotropy. *Cryst. Growth Des.* **2023**, *23*, 5137–5143. [CrossRef]
38. Zhong, R.; Guo, S.; Nguyen, L.T.; Cava, R.J. Frustrated spin-1/2 Dimer Compound $K_2Co_2(SeO_3)_3$ with Easy-axis Anisotropy. *Phys. Rev. B* **2020**, *102*, 224430. [CrossRef]
39. *Apex3*; Bruker AXS Inc.: Madison, WI, USA, 2015.
40. Sheldrick, G.M. A Short History of SHELX. *Acta Crystallogr. Sect. A Found. Crystallogr.* **2008**, *64*, 112–122. [CrossRef]
41. Asai, T.; Kiriyama, R. Optical and Magnetic Studies of $CuSeO_3$ $2H_2O$ Based on the Refined Crystal Structure. *Bull. Chem. Soc. Jpn.* **1973**, *46*, 2395–2401. [CrossRef]
42. Shanno, R.D. Revised Effective Ionic Radii and Systematic Studies of Interatomie Distances in Halides and Chaleogenides. *Acta Cryst.* **1976**, *A32*, 751–767. [CrossRef]
43. Amuneke, N.G.; Gheorghe, D.E.; Lorenz, B.; Möller, A. Synthesis, Crystal Structure, and Physical Properties of $BaAg_2Cu[VO_4]_2$: A New Member of the S = 1/2 Triangular Lattice. *Inorg. Chem.* **2011**, *50*, 2207–2214. [CrossRef]
44. Zhang, S.; Guo, W.; Yang, M.; Tang, Y.; Cui, Y.; Wang, N.; He, Z. A frustrated Ferrimagnet $Cu_5(VO_4)_2(OH)_4$ with a 1/5 Magnetization Plateau on a New Spin-lattice of Alternating Triangular and Honeycomb Strips. *Dalton Trans.* **2015**, *44*, 20562–20567. [CrossRef]

45. Kakarla, D.C.; Yang, Z.H.; Wu, H.C.; Kuo, T.W.; Tiwari, A.; Li, W.-H.; Lee, C.H.; Wang, Y.-Y.; Lin, J.-Y.; Chang, C.K.; et al. Single Crystal Growth and Structural, Magnetic, and Magnetoelectric Properties in Spin-Frustrated bow-tie Lattice of α-$Cu_5O_2(SeO_3)_2Cl_2$. *Mater. Adv.* **2021**, *2*, 7939–7948. [CrossRef]
46. He, Z.; Lin, C.; Cheng, W.; Okazawa, A.; Kojima, N.; Yamaura, J.; Ueda, Y. Unusually Large Magnetic Anisotropy in a CuO-Based Semiconductor $Cu_5V_2O_{10}$. *J. Am. Chem. Soc.* **2011**, *133*, 1298–1300. [CrossRef]
47. Yang, M.; Zhang, S.; Guo, W.; Tanga, Y.; He, Z. Spin-frustration in a New Spin-1/2 Oxyfluoride System ($Cu_{13}(VO_4)_4(OH)_{10}F_4$) Constructed by Alternatively Distorted Kagome-like and Triangular Lattices. *Dalton Trans.* **2015**, *44*, 15396–15399. [CrossRef]
48. Ramirez, A.P. Strongly geometrically frustrated magnets. *Annu. Rev. Mater. Sci.* **1994**, *24*, 453–480. [CrossRef]
49. Mustonen, O.; Vasala, S.; Mutch, H.; Thomas, C.I.; Stenning, G.B.G.; Baggio-Saitovitch, E.; Cussen, E.J.; Karppinen, M. Magnetic Interactions in the $S = 1/2$ Square-lattice Antiferromagnets Ba_2CuTeO_6 and Ba_2CuWO_6: Parent Phases of a Possible Spin Liquid. *Chem. Commun.* **2019**, *55*, 1132–1135. [CrossRef] [PubMed]
50. Cheng, J.; Tian, W.; Zhou, J.; Lynch, V.M.; Steinfink, H.; Manthiram, A.; May, A.F.; Garlea, V.A.; Neuefeind, G.C.; Yan, J. Crystal and Magnetic Structures and Physical Properties of a New Pyroxene $NaMnGe_2O_6$ Synthesized under High Pressure. *J. Am. Chem. Soc.* **2013**, *135*, 2776–2786. [CrossRef] [PubMed]
51. Vasiliev, A.N.; Ignatchik, O.L.; Sokolov, A.N.; Hiroi, Z.; Isobe, M.; Ueda, Y. Long-range Magnetic Order in Quasi-one-dimensional Chromium-based ($S = 3/2$) pyroxene $(Li,Na)Cr(Si,Ge)_2O_6$. *Phys. Rev. B* **2005**, *72*, 012412. [CrossRef]